Int. J. Electrochem. Sci., 12 **(2017)** 6506 – 6519, doi: 10.20964/2017.07.47

International Journal of
ELECTROCHEMICAL
SCIENCE
www.electrochemsci.org

Effect of Yttrium Addition on Corrosion Resistance of Zr-based Bulk Metallic Glasses in NaCl Solution

Liusi Yu[1], *Junlei Tang*[1,*], *Jichao Qiao*[2], *Hu Wang*[3], *Yingying Wang*[1], *Mihai Apreutesei*[4], *Mohammad Chamas*[1], *Ming Duan*[1]

[1] School of Chemistry and Chemical Engineering, Southwest Petroleum University, Chengdu 610500, P.R. China
[2] School of Mechanics, Civil Engineering and Architecture, Northwestern Polytechnical University, Xi'an 710072, P.R. China
[3] School of Material Science and Engineering, Southwest Petroleum University, Chengdu 610500, P.R. China
[4] Université de Lyon, Institut des Nanotechnologies de Lyon INL-UMR5270, CNRS, Ecole Centrale de Lyon, Ecully F-69134, France
[*]E-mail: tangjunlei@126.com

Received: 11 April 2017 / *Accepted:* 2 May 2017 / *Published:* 12 June 2017

This study investigated the effect of yttrium addition on the electrochemical properties of $(Zr_{58}Nb_3Cu_{16}Ni_{13}Al_{10})_{100-x}Y_x$ (x = 0, 0.5, 2.5 at.%) bulk metallic glasses in 3.5 wt.% NaCl solution. Electrochemical measurements, scanning electron microscopy (SEM), energy dispersive spectroscopy (EDS) and X-ray photoelectron spectroscopy (XPS) were employed. Zr-based bulk metallic glasses exhibited good corrosion resistance. It was ascribed to the formation of a protective passive film which was composed of ZrO_2, Al_2O_3 and a few oxides of other alloying elements, i.e. Y_2O_3. However, the breakdown potential decreased due to the addition of yttrium. Electrochemical impedance spectroscopy (EIS) suggested that yttrium addition could decrease the charge transfer resistance. That is, the addition of yttrium was harmful to the corrosion resistance of this Zr-based bulk metallic glass in 3.5 wt.% NaCl solution. It was attributed to the precipitation of Cu-Y richly quasi-crystal phase owing to yttrium addition, which caused inhomogeneous distribution of copper and yttrium in microstructure.

Keywords: Zr-based bulk metallic glasses; Pitting corrosion resistance; Yttrium; Electrochemical measurements; XPS

1. INTRODUCTION

Bulk metallic glasses (BMGs) formed by rapidly quenched from metallic alloy melts are amorphous in view of structure. BMGs have excellent physical and chemical properties such as high strength, large plastic limit and corrosion resistance [1-5]. Outstanding corrosion resistance of BMGs is attributed to their chemical and structural homogeneous, which are absence of grain boundaries, dislocations and other crystalline defects [6-8]. Due to these well-known properties, BMGs have attracted considerable attention and many multi-component BMGs have been developed, for example Ti-Zr-Cu-Pd [2], Co-Fe-Ta-B [9], Zr-Cu-Al-Ni [10], Fe-Cr-Mo-C-B [11], Cr-Co-Nb-B [12], La-Ni-Al [13], Cu-Zr-Al-Y [14], Al-Ni-Y [15], Ni-Nb-Zr [16], Mg-Cu-Ni-Ga [17] BMGs.

Zr-based BMGs are widely recommended due to their excellent glass-forming ability (GFA) with a wide super-cooled liquid region and good corrosion resistance in different corrosive medium. For instance, Kawashima et al. [18] reported that $Zr_{70}Cu_6Al_8Ni_{16}$ BMG passivated spontaneously in naturally aerated 0.5 M NaCl solution at 30°C. Huang et al. [19] found that $(Zr_{55}Al_{10}Cu_{50}Ni_5)_{99}Y_1$ BMG exhibited good bio-corrosion resistance in a phosphate-buffered saline. Li et al. [1] reported that $Zr_{56}Ni_{25-x}Al_{15}Nb_4Cu_x$ (x = 0 – 15 at.%) showed excellent corrosion resistance in H_2SO_4, HCl and NaCl solutions. Gebert et al. [10] also discovered that the bulk amorphous Zr-Cu-Al-Ni alloy showed strong passivation behavior in a 0.1 M Na_2SO_4 (pH = 8) electrolyte and the strong protective surface layers formed by anodization.

It has been reported that adding a small amount of yttrium could improve the GFA, thermal stability and mechanical properties of BMGs [20-22]. The effects of yttrium on the corrosion behavior of BMGs are also greatly considered. Addition of yttrium showed different influence on the corrosion resistance of BMGs in various corrosive media. Wang et al. [11] reported that in 1 mol/L HCl solution, 0.5 at.% yttrium addition exhibited a detrimental effect on corrosion resistance of Fe-Cr-Mo-B BMGs while more yttrium additions have a beneficial effect. Wang et al. [23] found similar results for $Fe_{50-x}Cr_{15}Mo_{14}C_{15}B_6Y_x$ bulk amorphous steels. It was explained by that the structural defects in passive films were changed by additions of yttrium. Liu et al. [24] pointed out that crystalline phase would precipitate when yttrium addition exceeds 3 at.% and addition of yttrium element was deteriorative for $Cu_{50}Zr_{45}Al_5$ metallic glass in 3.5 wt.% NaCl solution. However, Wang et al. [25] reported that yttrium doping could improve bio-corrosion resistance of $Mg_{69}Zn_{27}Ca_4$ bulk metallic glass in simulated body fluid at 37°C. He et al. [26] obtained results essentially in agreement with Wang et al.. They found that Mg-Zn-Mn alloys showed high corrosion resistance in Hank′s solution and the XPS results revealed this was attributed to the formation of Y_2O_3 protective passive film. Even a lot papers have emphasized the role of yttrium in corrosion of BMG, however, no systematic study about the effect of yttrium addition on corrosion behavior of Zr-based BMG was conducted.

To probe the effect of yttrium addition on the corrosion resistance of Zr-based BMG, the material used in this study had a nominal composition of $Zr_{58}Nb_3Cu_{16}Ni_{13}Al_{10}$ and its dynamic mechanical and thermo-mechanical properties were investigated [27]. We added different contents of yttrium into $Zr_{58}Nb_3Cu_{16}Ni_{13}Al_{10}$ BMG and investigated its effect on pitting corrosion by electrochemical techniques and X-ray photoelectron spectroscopy.

2. EXPERIMENTAL

Master alloys of Zr-based bulk metallic glass with nominal composition $(Zr_{58}Nb_3Cu_{16}Ni_{13}Al_{10})_{100-x}Y_x$ (x = 0, 0.5, 2.5 at.%) were prepared in melting equipment. The ingots of

$(Zr_{58}Nb_3Cu_{16}Ni_{13}Al_{10})_{100-x}Y_x$ (x = 0, 0.5, 2.5 at.%) alloys were prepared by arc-melting pure Zr, Nb, Cu, Ni, Al and Y in a Ti-gettered argon atmosphere. To ensure the homogeneity of the samples, the ingots were re-melted four-times and cast into a copper mold under pressure of high-purity argon to produce plates. The size of rectangular-plate was 30 mm (length) × 5 mm (width) × 3 mm (thickness).

The amorphous structure of as-cast Zr-based BMGs was characterized by X-ray diffraction (XRD, X Pert PRO MPD) with Cu Kα radiation.

Electrochemical measurements were performed using a CS350 electrochemical system at room temperature in a conventional three-electrode cell in aerated 3.5 wt.% NaCl solution. A saturated calomel electrode (SCE) was used as the reference electrode (E_{SCE} = 241 mV, SHE) and platinum as the counter electrode. Zr-based BMGs, as the working electrode, were ground with SiC papers of up to 5000 grit, and then ultrasonically cleaned in alcohol, finally cleaned by deionized water. The working electrode was connected into the cell by copper wire and sealed by resin with an exposed area 0.4 cm^2. Prior to electrochemical measurements, samples were exposed to air for 36 hours after grinding.

Potentiodynamic polarization curves were conducted with a scan rate of 0.5 mV/s. Electrochemical impedance spectroscopy (EIS) was performed under open circuit potential (OCP) over a frequency range from 100 kHz to 10 mHz, with a sinusoidal potential perturbation of ±10 mV amplitude. The impedance plots were interpreted on the basis of electrical equivalent circuits using ZSimpWin software. Before polarization and EIS tests, OCP was monitored about 900 s to obtain a steady state.

Scanning electron microscopy (SEM, EVO MA15 ZEISS) coupled with energy dispersive spectroscopy (EDS, X-MaxN OXFORD INSTRUMENTS) detector was used to characterize the surface morphologies after polarization. Samples were immersed in 3.5 wt.% NaCl solution for 24 hours and the compositions of passive film formed on the surface of metallic glasses were analyzed with X-ray photoelectron spectroscopy (XPS) using an ESCALAB250 (THERMO VG, USA) photoelectron spectrometer equipped with Al-Kα (1486.6 eV) source. From the spectra, the chemical compositions of passive films were quantitatively determined using sensitivity factor.

3. RESULTS AND DISCUSSION

3.1. Microstructure characterization

Prior to electrochemical measurements, the microstructures of as-cast Zr-based BMGs were confirmed by X-ray diffraction. Fig. 1 shows the XRD patterns of as-cast $(Zr_{58}Nb_3Cu_{16}Ni_{13}Al_{10})_{100-x}Y_x$ (x = 0, 0.5, 2.5 at.%) BMGs. Each curve only exhibits broad diffraction humps, which are typical features of the amorphous structure.

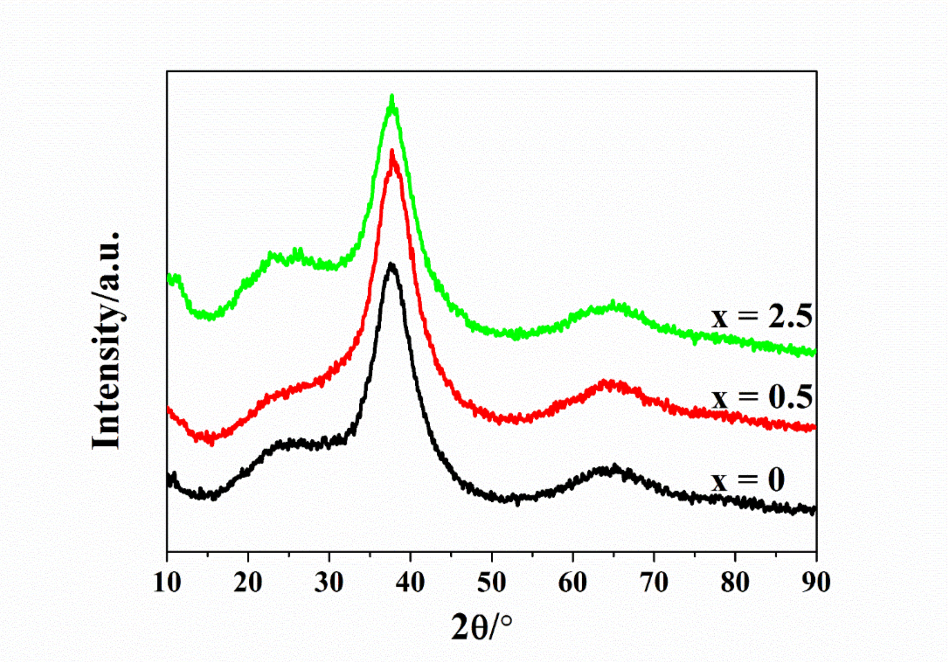

Figure 1. XRD patterns of $(Zr_{58}Nb_3Cu_{16}Ni_{13}Al_{10})_{100-x}Y_x$ (x = 0, 0.5, 2.5 at.%) BMGs.

3.2. Electrochemical properties

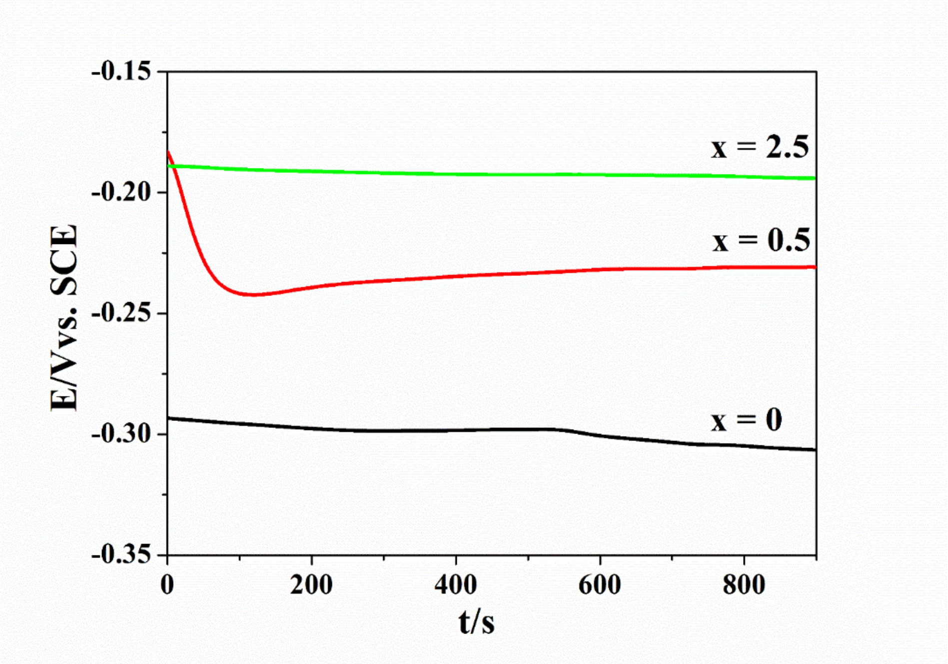

Figure 2. Open circuit potential of $(Zr_{58}Nb_3Cu_{16}Ni_{13}Al_{10})_{100-x}Y_x$ (x = 0, 0.5, 2.5 at.%) BMGs in aerated 3.5 wt.% NaCl solution at room temperature.

The OCP evolutions of these Zr-based BMGs in 3.5 wt.% NaCl solution at room temperature are illustrated in Fig. 2. During immersion process, the OCP of $Zr_{58}Nb_3Cu_{16}Ni_{13}Al_{10}$, $(Zr_{58}Nb_3Cu_{16}Ni_{13}Al_{10})_{99.5}Y_{0.5}$ and $(Zr_{58}Nb_3Cu_{16}Ni_{13}Al_{10})_{97.5}Y_{2.5}$ BMGs remained stable recording values about -0.30 V, -0.23 V and -0.19 V in a short time, respectively. These results can be considered as a steady state of the electrochemical behavior for the considered period that is suitable to confirm the electrochemical properties.

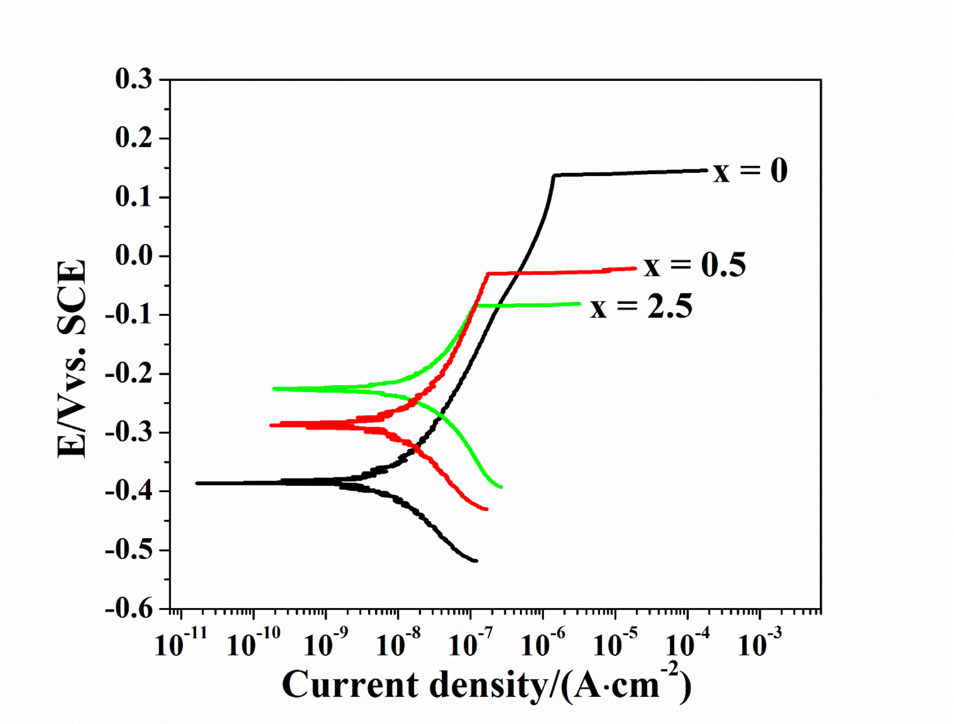

Figure 3. Potentiodynamic polarization curves of $(Zr_{58}Nb_3Cu_{16}Ni_{13}Al_{10})_{100-x}Y_x$ (x = 0, 0.5, 2.5 at.%) BMGs in aerated 3.5 wt.% NaCl solution at room temperature.

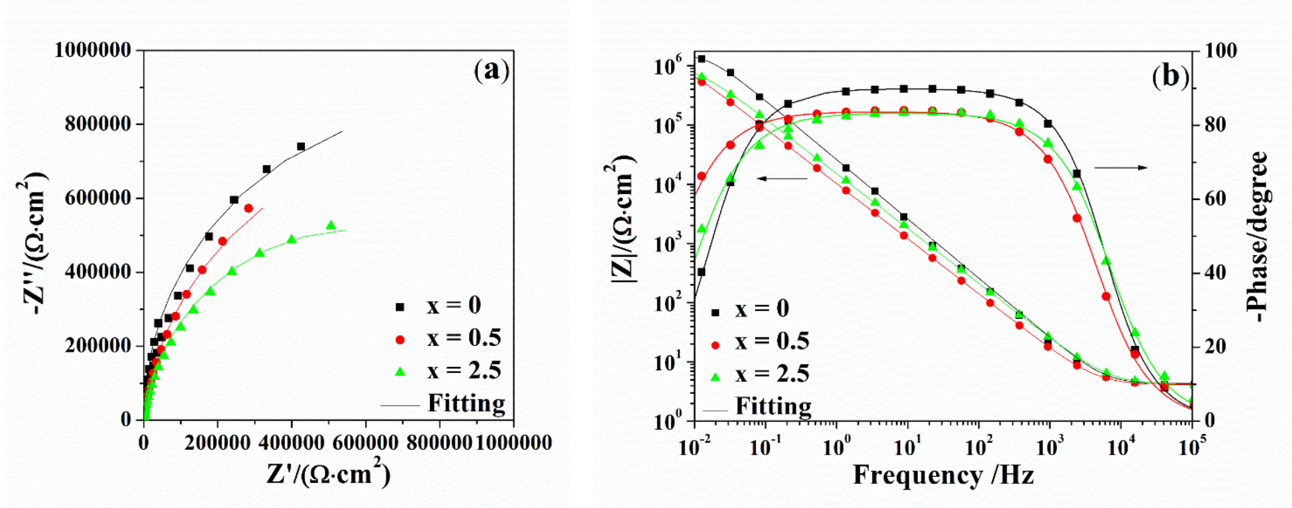

Figure 4. EIS plots of $(Zr_{58}Nb_3Cu_{16}Ni_{13}Al_{10})_{100-x}Y_x$ (x = 0, 0.5, 2.5 at.%) BMGs recorded at room temperature in aerated 3.5 wt.% NaCl solution: (a) Nyquist plot; (b) Bode plot.

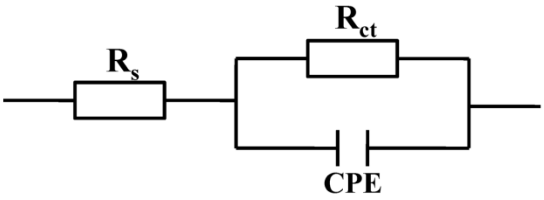

Figure 5. Equivalent electrical circuit diagram used to fit the EIS data.

The potentiodynamic polarization curves of Zr-based BMGs in 3.5 wt.% NaCl solution are displayed in Fig. 3. It is clear that all of the Zr-based BMGs passivated spontaneously. Their anodic current densities were very low (10^{-8} – 10^{-7} $A \cdot cm^{-2}$) and increased slowly with the increase of anodic potential. When the anodic potential reached a critical value, the anodic current density sharply increased, implying the occurrence of pitting corrosion in a localized region. Related electrochemical parameters are listed in Table 1. It is noted that the corrosion potential (E_{corr}) shifted to a positive direction and the corrosion current density (i_{corr}) also increased from 2.4×10^{-9} A/cm^2 to 3.5×10^{-9} A/cm^2 as the yttrium content increased. The breakdown potential (E_b) is 0.14 V for $Zr_{58}Nb_3Cu_{16}Ni_{13}Al_{10}$ BMG, -0.02 V for $(Zr_{58}Nb_3Cu_{16}Ni_{13}Al_{10})_{99.5}Y_{0.5}$ BMG and -0.08 V for $(Zr_{58}Nb_3Cu_{16}Ni_{13}Al_{10})_{97.5}Y_{2.5}$ respectively. The difference between (E_b - E_{corr}) (passivation range) also decreased with the increase of yttrium content. It indicates that pitting corrosion susceptibility of Zr-based BMGs in 3.5 wt.% NaCl solution increased with yttrium addition. Similar results were reported by Liu et al. [24] that the addition of yttrium can deteriorate the corrosion resistance of $Cu_{50}Zr_{45}Al_5$ metallic glass in 3.5 wt.% NaCl solution.

Table 1. Electrochemical parameters of polarization curves for $(Zr_{58}Nb_3Cu_{16}Ni_{13}Al_{10})_{100-x}Y_x$ (x = 0, 0.5, 2.5 at.%) BMGs in aerated 3.5 wt.% NaCl solution

Samples	E_{corr} (V)	i_{corr} (A/cm^2)	E_b (V)	E_b-E_{corr} (V)
x = 0	-0.38	2.4×10^{-9}	0.14	0.52
x = 0.5	-0.29	3.5×10^{-9}	-0.02	0.27
x = 2.5	-0.22	4.5×10^{-9}	-0.08	0.14

Table 2. Equivalent circuit parameters of EIS results for $(Zr_{58}Nb_3Cu_{16}Ni_{13}Al_{10})_{100-x}Y_x$ (x = 0, 0.5, 2.5 at.%) BMGs in aerated 3.5 wt.% NaCl solution

Samples	R_s (Ω cm^2)	R_{ct} (Ω cm^2)	Q (Ω^{-1} cm^{-2} s^n)	n
x = 0	4.347	1.674×10^6	5.411×10^{-6}	0.9998
x = 0.5	4.076	1.667×10^6	17.58×10^{-6}	0.9314
x = 2.5	4.154	1.113×10^6	11.99×10^{-6}	0.9276

Nyquist and Bode diagrams of Zr-based BMGs are represented in Fig. 4. Nyquist plots (Fig.4a) exhibited a semicircle with only a time constant on Bode diagram (Fig.4b), implying the formation of protective and compact passive film. The Bode plots are composed of three parts: (I) at high frequency region, the phase angle closes to 0°, related impedance represents the solution resistance; (II) at medium frequency region (10^3 Hz – 10^0 Hz) the phase angle closes to 80°, corresponding to the capacitive behavior; (III) at low frequency region (10^0 Hz – 10^{-2} Hz), the absolute impedance value stands for the corrosion impedance [28]. The absolute impedance decreased with the addition of yttrium, especially in the low frequency range, indicating that the corrosion impedance decreased. EIS plots in 3.5 wt.% NaCl solution have been interpreted by the equivalent electric circuit showed in Fig. 5, which consists of the solution resistance (R_s), the charge transfer resistance (R_{ct}) and the capacitance of a constant phase element (CPE). R_{ct} corresponding to the charge transfer in electrode/electrolyte interface is dominated by the impedance of passive film [7]. CPE represents a non-ideal capacitance behavior of electrode/electrolyte interface, corresponding to inhomogeneous rough and porous surface [29]. The impedance of CPE is determined by the following equation:

$Z_{CPE} = Q^{-1} (j\omega)^{-n}$ (1)

Where n = 1 represents a perfect capacitance, n = 0.5 represents a Warburg resistance, n = 0 represents a resistance [30]. Corresponding electrochemical parameters are given in Table 2.

From the Table 2, the n values are closed to 1, confirming that the BMG samples have capacitive behavior characterized by a double layer and the space charge region at the interface according to homogenous passive film. However, it can be noted that the n value of CPE decreased with the addition of yttrium, indicating that yttrium appeared to be harmful to surface homogeneity. R_{ct} values decreased due to the yttrium addition, implying the corrosion of the BMGs with more yttrium addition occurred more easily.

3.3. Corrosion morphology

The surface morphologies of the Zr-based BMGs have been examined by SEM after potentiodynamic polarization tests. It is no doubt that the surface of Zr-based BMGs endured corrosion attacks by Cl^- ions that the passive film has been broken in a localized area after anodic polarization, and the SEM micrographs of the corroded area are shown in Fig. 6.

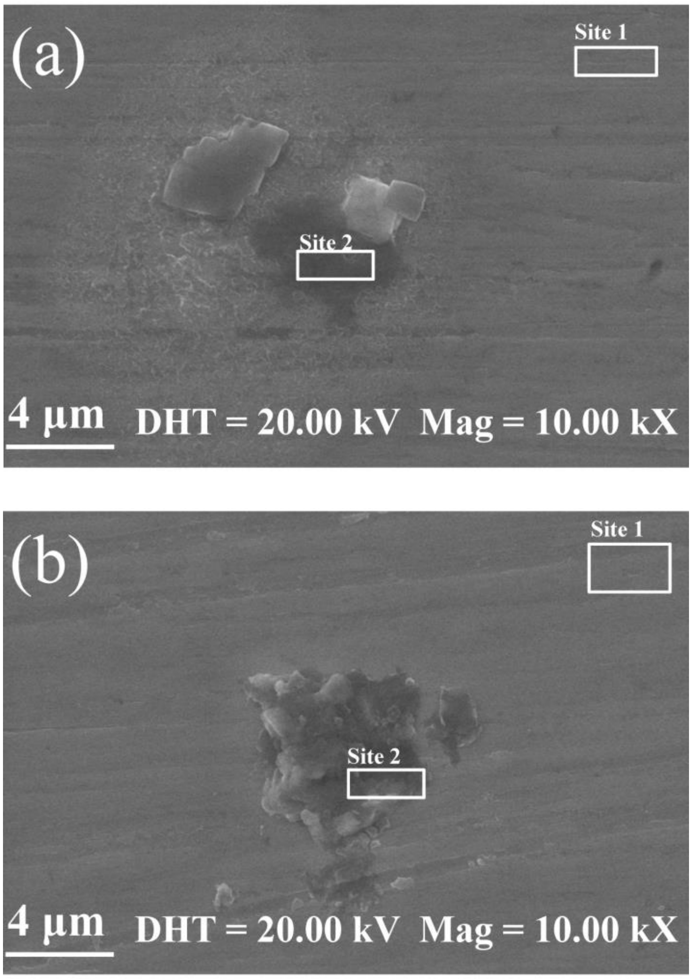

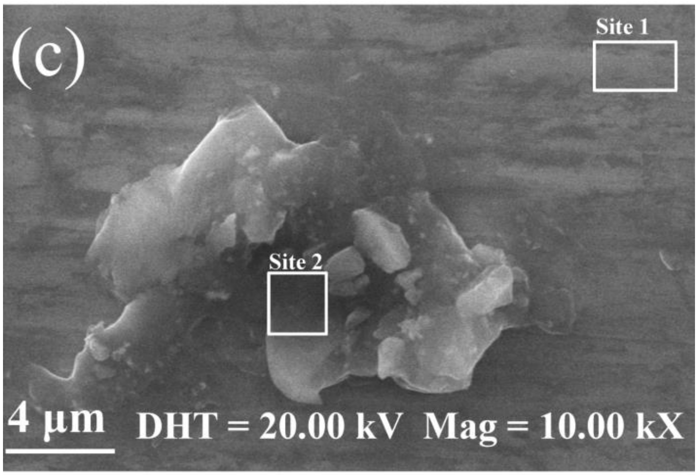

Figure 6. SEM morphologies of $(Zr_{58}Nb_3Cu_{16}Ni_{13}Al_{10})_{100-x}Y_x$ (x = 0, 0.5, 2.5 at.%) BMGs after potentiodynamic polarization scan recorded at room temperature in aerated 3.5 wt.% NaCl: (a) $Zr_{58}Nb_3Cu_{16}Ni_{13}Al_{10}$; (b) $(Zr_{58}Nb_3Cu_{16}Ni_{13}Al_{10})_{99.5}Y_{0.5}$; (c) $(Zr_{58}Nb_3Cu_{16}Ni_{13}Al_{10})_{97.5}Y_{2.5}$.

Table 3. EDS results of corrosion sites and matrix for $(Zr_{58}Nb_3Cu_{16}Ni_{13}Al_{10})_{100-x}Y_x$ (x = 0, 0.5, 2.5 at.%) BMGs after polarization test in 3.5 wt.% NaCl solution

Composition	x = 0		x = 0.5		x = 2.5	
(at.%)	Site 1	Site 2	Site 1	Site 2	Site 1	Site 2
Zr	54.1	51.5	53.3	39.7	51.5	40.3
Al	7.4	7.0	7.5	8.3	7.5	5.8
Cu	16.3	15.8	16.7	13.5	15.4	11.9
Ni	13.8	13.2	13.8	10.8	13.2	9.3
Nb	3.5	3.7	3.8	3.5	2.7	2.9
Y	–	–	0.5	1.5	2.5	6.5
O	4.9	8.8	4.4	22.7	7.2	23.3

The corrosion morphology of all samples showed that the occluded pitting sites were covered by corrosion products.

The chemical compositions of corrosion sites and matrix after polarization test in 3.5 wt.% NaCl solution measured by EDS are summarized in Table 3. The EDS chemical composition of yttrium-free BMG was very similar for both corrosion sites and matrix. However, distribution of elements became different with yttrium addition, especially in terms of yttrium content which was higher in the corrosion sites. Such result reveals that the localized corrosion exhibited an yttrium enrichment of corrosion products.

3.4. X-ray photoelectron spectroscopy characterization

Fig. 7 presents the XPS analysis performed to clarify the compositions of passive layer for Zr-based BMGs after immersion in 3.5 wt.% NaCl solution for 24 hours under the corrosion potential. The binding energies of zirconium, niobium, copper, nickel, aluminum, yttrium, oxygen were interpreted according to NIST XPS database, and the C_{1s} peak (284.6 eV) was used as the reference to correct the charging shifts.

Peaks of Zr 3d 5/2 (181.8 eV) and Zr 3d 3/2 (184.19 eV) observed in the Zr 3d spectrum corresponds to ZrO_2. The peaks at 73.61 eV and 76.18 eV binding energies are assigned to 2p 3/2 and 2p 1/2 of Al 2p spectrum, originating from Al_2O_3. The Nb spectrum is composed of 3d 5/2 (206.80 eV) and 3d 3/2 (209.45 eV) originating from Nb_2O_5 and the peaks at 204.80 eV and 202.14 eV binding energies are assigned to NbO and Nb respectively.

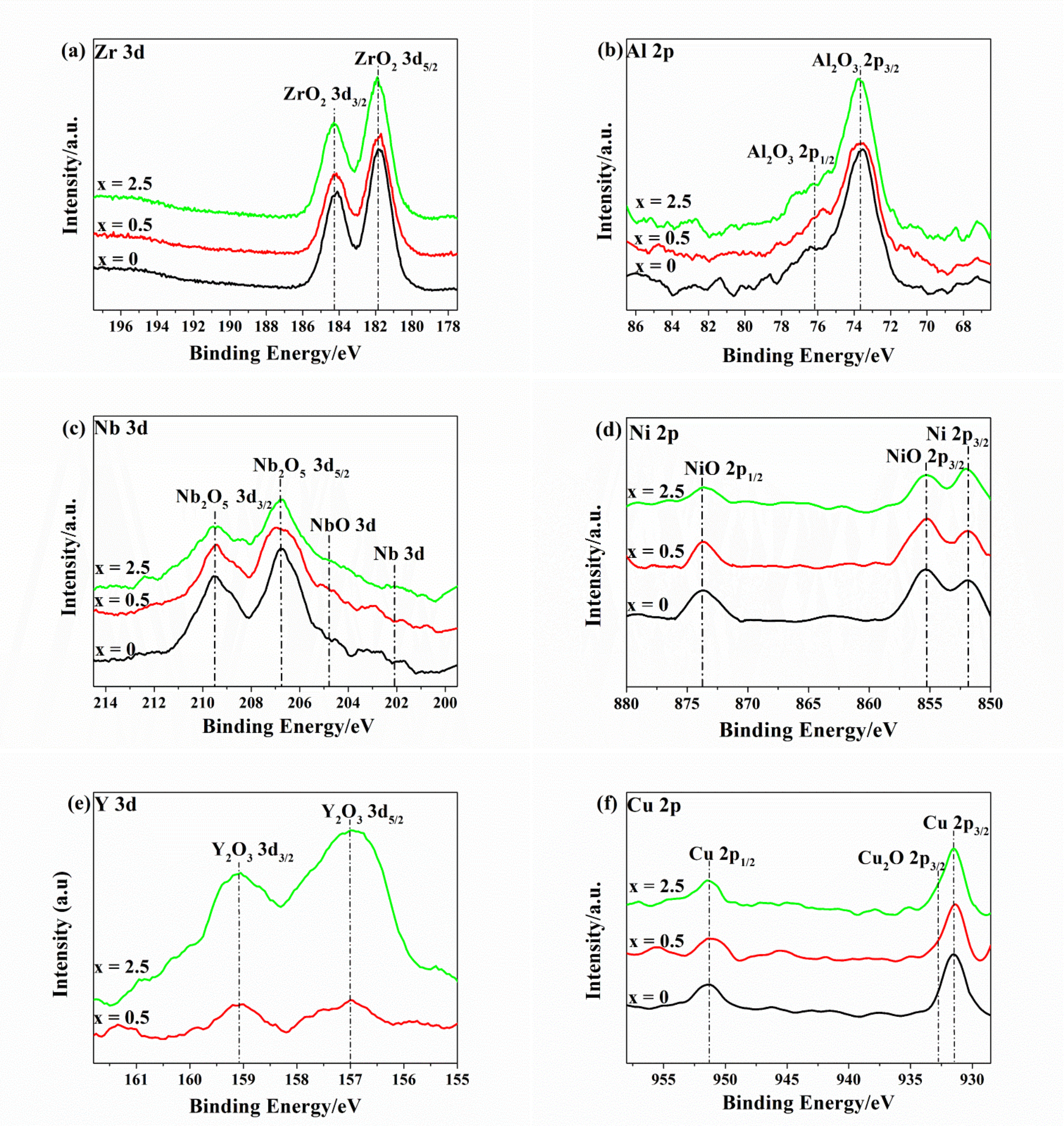

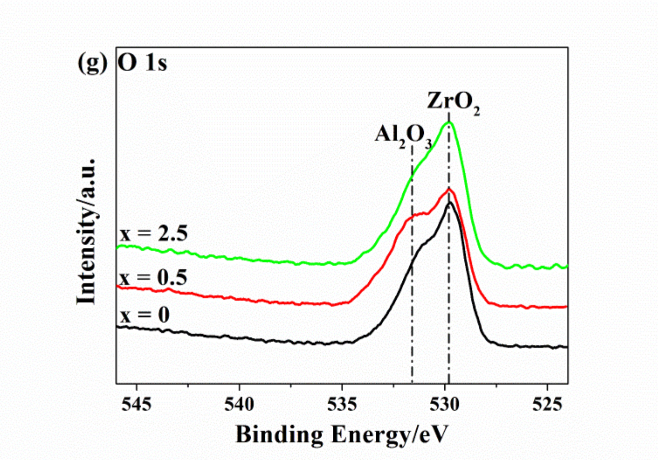

Figure 7. The XPS spectra of passive films formed on $(Zr_{58}Nb_3Cu_{16}Ni_{13}Al_{10})_{100-x}Y_x$ (x = 0, 0.5, 2.5 at.%) BMGs after immersion in aerated 3.5 wt.% NaCl solution at room temperature for 24 h: (a) Zr 3d; (b) Al 2p; (c) Nb 3d; (d) Ni 2p; (e) Y 3d; (f) Cu 2p; (g) O1s.

In Ni 2p spectrum, the peak located at 851.90 eV belongs to Ni 2p 3/2, while the peaks at 855.50 eV and 873.48 eV are assigned to Ni 2p 3/2 and Ni 2p 1/2 originating from NiO. For $(Zr_{58}Nb_3Cu_{16}Ni_{13}Al_{10})_{99.5}Y_{0.5}$ and $(Zr_{58}Nb_3Cu_{16}Ni_{13}Al_{10})_{97.5}Y_{2.5}$ BMGs, the Y 3d spectrum consists of two peaks by multiplet splitting (3d 5/2 and 3d 3/2 at 157.00 eV and 159.22 eV binding energies) that belongs to Y_2O_3.

Table 4. The composition (at.%) of passive film calculated from XPS for the $(Zr_{58}Nb_3Cu_{16}Ni_{13}Al_{10})_{100-x}Y_x$ (x = 0, 0.5, 2.5 at. %) BMGs after immersion in aerated 3.5 wt.% NaCl solution for 24 hours

Composition (at.%)	x = 0	x = 0.5	x = 2.5
ZrO_2	57.00	54.29	55.77
Al_2O_3	33.22	35.97	32.58
Y_2O_3	–	0.20	2.37
Ni	0.61	0.73	1.13
NiO	2.18	1.82	1.89
Nb	0.21	0.30	0.13
NbO	0.37	0.49	0.91
Nb_2O_5	4.60	5.16	3.86
Cu	1.83	0.88	1.11
Cu_2O	–	0.17	0.24

On Cu 2p spectrum, the peaks at 931.20 eV and 951.20 eV are fitted with the metallic state of copper (Cu). The peak at 932.50 eV originating from Cu_2O is observed on the surface film of $(Zr_{58}Nb_3Cu_{16}Ni_{13}Al_{10})_{99.5}Y_{0.5}$ and $(Zr_{58}Nb_3Cu_{16}Ni_{13}Al_{10})_{97.5}Y_{2.5}$ BMGs.

Peaks of O1s spectra are mainly composed of two peaks located at 529.90 eV and 531.60 eV binding energies originating from ZrO_2 and Al_2O_3, respectively.

Table 4 shows the composition of passive film formed in 3.5 wt.% NaCl solution. The results prove that all elements of the Zr-based BMGs exist in the passive layer. However, the content of nickel and copper substantially decreased after immersion. The concentrations of ZrO_2 and Al_2O_3 in the passive layer for $Zr_{58}Nb_3Cu_{16}Ni_{13}Al_{10}$, $(Zr_{58}Nb_3Cu_{16}Ni_{13}Al_{10})_{99.5}Y_{0.5}$ and $(Zr_{58}Nb_3Cu_{16}Ni_{13}Al_{10})_{97.5}Y_{2.5}$ BMGs reach up to 90.22 at.%, 90.26 at.% and 88.35 at.%, respectively. Hence, the corrosion resistance of the Zr-based BMGs exhibited a decreasing tendency but still presented good corrosion resistance.

3.5. The role of yttrium

The corrosion resistance of the Zr-based BMGs are highly depends on the individual element of the BMGs [31]. Their standard equilibrium electrode potentials are useful to predict the individual electrochemical behavior in different corrosive mediums. The standard equilibrium electrode potential of Y, Al, Zr and Nb is -2.61 V_{SCE} ,-1.90 V_{SCE}, -1.77 V_{SCE} and -1.34 V_{SCE}, respectively [32]. Therefore, it is reasonable that Y, Al, Zr and Nb would preferentially be oxidized and be beneficial to the corrosion resistance in virtue of the high stability of their corresponding oxides in aqueous media [31,33,34]. Ni and Cu have relatively higher standard equilibrium electrode potential values of -0.49 V_{SCE} and 0.01 V_{SCE} [32]. Especially considering Cu has the highest standard equilibrium electrode potential among these six elements, it could accelerate the pitting corrosion in $(Zr_{58}Nb_3Cu_{16}Ni_{13}Al_{10})_{100-x}Y_x$.

Cu would enhance the galvanic coupling effect and thus the dissolution of amorphous matrix was accelerated in $Zr_{70}Cu_6Al_8Ni_{16}$ BMG and $Zr_{59}Ti_3Cu_{20}Al_{10}Ni_8$ BMG in Cl-ion-containing solution [18,35]. The similar mechanism was proposed in $Zr_{58}Cu_{28}Al_{10}Ti_4$ amorphous alloy in 0.5 M NaCl solution, that Cu provided favorable galvanic effect for rapid preferential dissolution of active metals like Zr, Ti and Al [36]. Li et al. [37] pointed out that more replacement of Cu by Ni in $Zr_{60}Cu_{25-x}Al_{15}Ni_x$ (x = 0, 15 and 25) BMGs could improve the corrosion resistance in 3 wt.% NaCl solution, that is, the BMGs containing less Cu would show better corrosion resistance in NaCl solution.

In another hand, Yang et al. [38] reported that the interaction between yttrium and copper is stronger than the one between zirconium and copper by theoretically calculation with real-place recursion method. The yttrium and copper combination could promote the precipitation tendency of Cu-Y richly quasi-crystal phase. Thus, with the presence of yttrium, the localized inhomogeneity of copper is facilitated and the distribution of yttrium itself becomes heterogeneous as well. These microstructural heterogeneities contribute to heterogeneities in the passive film.

From the XPS results, we can see that the compositions of passive films are mainly composed of ZrO_2 and Al_2O_3 which are protective with high compactness. It is well known that yttrium not only can promote the passivation of other elements, but is capable also to form a stable Y_2O_3 passive film with high thermodynamic stability [34]. Hence, all Zr-based BMGs in our study exhibited high corrosion resistance with low free corrosion current densities. The lacking of nickel on the as prepared Zr-based BMG surface could be ascribed to surficial nickel is active in the solution containing Cl^- ions as reported in similar BMG system [34], but no obvious effect from different yttrium addition could be identified. The contents of copper (including metallic and oxidized states) are 1.83 at.% ($Zr_{58}Nb_3Cu_{16}Ni_{13}Al_{10}$), 1.05 at.% ($(Zr_{58}Nb_3Cu_{16}Ni_{13}Al_{10})_{99.5}Y_{0.5}$) and 1.35 at.% ($(Zr_{58}Nb_3Cu_{16}Ni_{13}Al_{10})_{97.5}Y_{2.5}$) and most of copper have dissolved after immersion. The residual copper mainly retains in the form of metallic state, however, for $(Zr_{58}Nb_3Cu_{16}Ni_{13}Al_{10})_{99.5}Y_{0.5}$ and $(Zr_{58}Nb_3Cu_{16}Ni_{13}Al_{10})_{97.5}Y_{2.5}$ samples low amounts of copper are oxidized into Cu_2O.

The formation of Cu_2O and dissolution of copper in 3.5 wt.% NaCl solution [39,40] can be described by equations (2) to (8). The oxygen reduction, which is the controlling step, always acts as the cathode reaction occurring on Cu in sodium chloride solution:

$$O_2 + 2H_2O + 4e^- \rightarrow 4OH^- \quad (2)$$

The anodic dissolution of copper in chloride solutions can be presented by the reaction:

$$Cu + OH^- \rightarrow Cu(OH)_{ads} + e^- \quad (3)$$

$$2Cu(OH)_{ad} \rightarrow Cu_2O + H_2O \quad (4)$$

The process is also controlled by oxidation reaction of dissolved oxygen is expressed as follows:

$$4Cu + O_2 \rightarrow 2Cu_2O \quad (5)$$

Then the complex reactions of chloride are expressed as follows:

$$Cu + Cl^- \rightarrow CuCl_{ads} + e^- \quad (6)$$

$$CuCl_{ads} + Cl^- \rightarrow CuCl_2^- \quad (7)$$

$$CuCl_2^- \rightarrow Cu^{2+} + 2Cl + e^- \quad (8)$$

In comparison to the nominal composition of copper, the copper contents in passive films are lower due to its preferential dissolution in 3.5 wt.% NaCl solution. Furthermore, it has been found that more copper is oxidized and dissolved. This indicates that the reaction activity of copper in these Zr-based BMGs is enhanced by the addition of yttrium. This could be explained by the inhomogeneous distributions of yttrium and copper elements owing to the addition of yttrium. With the yttrium–copper clusters, the localized corrosion could be initiated more easily. After anodic polarization, both yttrium and copper formed oxides, while more yttrium remained. This is why the EDS analysis (Fig. 6) shows that the content of yttrium is higher and the content of copper is lower in the corroded sites compared to in the matrix.

4. CONCLUSIONS

The effect of yttrium on the corrosion behavior of $(Zr_{58}Nb_3Cu_{16}Ni_{13}Al_{10})_{100-x}Y_x$ (x = 0, 0.5, 2.5 at.%) BMGs was investigated in 3.5 wt.% NaCl solution. Electrochemical measurements showed that the breakdown potential and impedance of the Zr-based BMGs decreased due to the yttrium addition. Chemical composition analysis showed that the yttrium was enrichment in the corrosion site. However, the protective passive films which mainly consist of ZrO_2 and Al_2O_3 can be formed on the both surfaces of the Zr-based BMGs with yttrium or without yttrium in 3.5 wt.% NaCl solution.

The addition of yttrium could accelerate the precipitation of copper-yttrium clusters in microstructure, which made an inhomogeneous distribution of copper and yttrium. These heterogeneities could increase pitting corrosion susceptibility which has been demonstrated from polarization curves and surface analyses. Hence, in 3.5 wt.% NaCl solution the corrosion resistance of the Zr-based BMGs decreased with the yttrium addition.

ACKNOWLEDGEMENTS

This investigation is financially supported by National Natural Science Foundation of China under grant Nos. 51401173, 51401192 and Foundation of Youth Science and Technology Innovation Team of Sichuan Province under grant No. 2015TD0007.

References

1. Y. Li, W. Zhang, F. Qin, A. Makino, *J. Alloy Compd.*, 615(2013) S71.
2. J. Fornell, N. Van Steenberge, a. Varea, E. Rossinyol, E. Pellicer, S. Suriñach, M. D. Baró, J. Sort, *J. Mech. Behav. Biomed.*, 4(2011) 1709.
3. S. Pang, T. Zhang, K. Asami, A. Inoue, *J. Mater. Res.*, 18(2003) 1652.
4. J. Kong, Z. Ye, W. Chen, X. Shao, K. Wang, Q. Zhou, *Mater. Design*, 88(2015) 69.
5. C. Zhang, X. Hui, X. Liu, G. Chen, *Rare Metal Mat. Eng.*, 37(2008) 320.
6. H. Kou, Y. Li, T. Zhang, J. Li, J. Li, T. *Nonferr. Metal Soc.*, 21(2011) 552.
7. D. P. Wang, S. L. Wang, J. Q. Wang, *Corros. Sci.*, 59(2012) 88.
8. S. González, E. Pellicer, S. Suriñach, M. D. Baró, J. Sort, *Intermetallics*, 28(2012) 149.
9. A. H. Taghvaei, J. Bednarik, J. Eckert, *Intermetallics*, 69(2016) 21.
10. A. Gebert, K. Buchholz, A. Leonhard, K. Mummert, J. Eckert, L. Schultz, *Mat. Sci. Eng. A,* 267(1999) 294.
11. Z. M. Wang, Y. T. Ma, J. Zhang, W. L. Hou, X. C. Chang, J. Q. Wang, *Electrochim. Acta*, 54(2008) 261.
12. J. J. Si, X. H. Chen, Y. H. Cai, Y. D. Wu, T. Wang, X. H. Hui, *Corros. Sci.*, 107(2016) 123.
13. J. C. Qiao, Y.-J. Wang, J. M. Pelletier, L. M. Keer, M. E. Fine, Y. Yao, *Acta Mater.*, 98(2015) 43.
14. D. Zander, B. Heisterkamp, I. Gallino, *J. Alloy Compd.*, 434–435(2007) 234.
15. S. F. Chen, S. L. Lin, J. K. Chen, Y. L. Lin, *Intermetallics*, 18(2010) 1954.
16. K. Zhang, X. Gao, Y. Dong, Q. Xing, Y. Wang, *J. Non-Cryst. Solids*, 425(2015) 46.
17. G. Y. Yuan, K. Amiya, A. Inoue, *J. Non-Cryst. Solids*, 351(2005), 729.
18. A. Kawashima, K. Ohmura, Y. Yokoyama, A. Inoue, *Corros. Sci.*, 53(2011) 2778.
19. L. Huang, D. Qiao, B. A. Green, P. K. Liaw, J. Wang, S. Pang, T. Zhang, *Intermetallics*, 17(2009) 195.
20. B. Li, J. Li, X. Fan, J. Chen, *Rare Metal Mat. Eng.*, 43(2014) 1558.
21. Y. Zhang, M. X. Pan, D. Q. Zhao, R. J. Wang, W. H. Wang, *Maters. Trans. JIM*, 41(2000) 1410.
22. J. Luo, H. Duan, C. Ma, S. Pang, T. Zhang, *Maters. Trans.*, 47(2006) 450.
23. Z. M. Wang, J. Zhang, X. C. Chang, W. L. Hou, J. Q. Wang, *Intermetallics*, 16(2008) 1036.
24. Y. Liu, Y. Wang, L. Xiao, M. Liu, Z. Shi, *Advanced Materials Research*, 851(2014) 62.
25. J. Wang, Y. Li, S. Huang, Y. Wei, X. Xi, K. Cai, F. Pan, *J. Mater. Sci. Technol.*, 30(2014) 1255.
26. W. He, E. Zhang, K. Yang, *Mat. Sci. Eng. C*, 30(2010) 167.
27. J. C. Qiao, S. Cardinal, J. M. Pelletier, H. Kato, *J. Alloy Compd.*, 628(2015) 357.
28. Q. Yu, C.F. Dong, Z.B. Liu, J.X. Liang, K. Xiao, X.G. Li, *Int. J. Electrochem. Sci.*, 10(2015) 2035.
29. B. Ter-Ovanessian, C. Alemany-Dumont, B. Normand, *Electrochim. Acta*, 133(2014) 373.
30. C. Boissy, C. Alemany-Dumont, B. Normand, *Electrochem. Commun.*, 26(2013) 10.
31. H.F. Tian, J.W. Qiao, H.J. Yang, Y.S. Wang, P.K. Liaw, A.D. Lan, *Appl. Surf. Sci.*, 363(2016) 37.
32. W. SHI, *WuHan University Press*, (2011) 304.
33. P.F. Gostin, D. Eigel, D. Grell, J. Eckert, E. Kerscher, A. Gebert. *J. Mater. Res.*, 30(2015) 283.
34. R. Jindal, V. S. Raja, M. A. Gibson, M. J. Styles, T. J. Bastow, C. R. Hutchinson, *Corros. Sci.*, 84(2014) 54.
35. A. Gebert, P.F. Gostin, L. Schultz, *Corros. Sci.*, 52(2010) 1711.
36. K. Mondal, B.S. Murty, U.K. Chatterjee, *Corros. Sci.*, 48(2006) 2212.
37. Y.H. Li, W. Zhang, C. Dong, J.B. Qiang, M. Fukuhara, A. Makino, A. Inoue, *Mat. Sci. Eng. A*.528(2011) 8851.

38. Y. Shuang, Z. Guo-ying, Z. Hui, *Journal of Shenyang Normal University (Natural Science Edition)*, 26(2008) 49.
39. P. Zhang, Q. Zhu, Q. Su, B. Guo, S. Cheng, *T. Nonferr. Metal. Soc.*, 26(2016) 1439.
40. H. Nady, M. M. El-rabiei, M. Samy, *Egyptian Journal of Petroleum*, 2016.